Tracking and Following a Tagged Leopard Shark with an Autonomous Underwater Vehicle

Christopher M. Clark
Department of Engineering, Harvey Mudd College, Claremont, California 91711
e-mail: clark@hmc.edu
Christina Forney and Esfandiar Manii
Department of Computer Science, Cal Poly State University, San Luis Obispo, California 93407
e-mail: cforney@calpoly.edu, emanii@calpoly.edu
Dylan Shinzaki
Department of Mechanical Engineering, Stanford University, Stanford, California 94305
e-mail: shinzaki@stanford.edu
Chris Gage
Department of Physics, Harvey Mudd College, Claremont, California 91711
e-mail: chris_gage@hmc.edu
Michael Farris and Christopher G. Lowe
Department of Biological Sciences, CSU Long Beach, Long Beach, California 90840
e-mail: mfarris@csulb.edu, clowe@csulb.edu
Mark Moline
School of Marine Science and Policy, University of Delaware, Lewes, Delaware 19958
e-mail: mmoline@udel.edu

Received 21 June 2012; accepted 17 January 2013

This paper presents a prototype system that enables an autonomous underwater vehicle (AUV) to autonomously track and follow a shark that has been tagged with an acoustic transmitter. The AUV's onboard processor handles both real-time estimation of the shark's two-dimensional planar position, velocity, and orientation states, as well as a straightforward control scheme to drive the AUV toward the shark. The AUV is equipped with a stereo-hydrophone and receiver system that detects acoustic signals transmitted by the acoustic tag. The particular hydrophone system used here provides a measurement of relative bearing angle to the tag, but it does not provide the sign (+ or −) of the bearing angle. Estimation is accomplished using a particle filter that fuses bearing measurements over time to produce a state estimate of the tag location. The particle filter combined with a heuristic-based controller allows the system to overcome the ambiguity in the sign of the bearing angle. The state estimator and control scheme were validated by tracking both a stationary tag and a moving tag with known positions. Offline analysis of these data showed that state estimation can be improved by optimizing diffusion parameters in the prediction step of the filter, and considering signal strength of the acoustic signals in the resampling stage of the filter. These experiments revealed that state estimate errors were on the order of those obtained by current long-distance shark-tracking methods, i.e., manually driven boat-based tracking systems. Final experiments took place in SeaPlane Lagoon, Los Angeles, where a 1-m leopard shark (*Triakis semifasciata*) was caught, tagged, and released before being autonomously tracked and followed by the proposed AUV system for several hours.

1. INTRODUCTION

The quantifying movement and habitat use behaviors of large highly mobile marine organisms have posed significant challenges for biologists. Recent advances in underwater technology have allowed for numerous studies in which individuals of particular species are captured, tagged, and tracked for extended periods of time. These studies provide position measurements as a function of time that yield insights into the daily and seasonal movement patterns of such species.

Currently, methods for tracking fish largely involve catching the fish and marking it with a satellite or acoustic transmitter tag. Satellite tags provide relatively accurate positional data (over scales of tens of meters to tens of kilometers) but only when the fish is at the surface (Voegeli et al., 2001). Acoustic tags can be tracked with an array of stationary receivers (passive tracking) or with a manually driven

Direct correspondence to: C. M. Clark, e-mail: clark@hmc.edu.

boat (active tracking) that requires a human to continuously position the boat to be within proximity of the fish and detect tag signals (Lowe and Bray, 2006; Sims et al., 2003). High-resolution positioning information can be extracted from static receiver arrays, but only if the fish remains within the local area of the receivers, which limits their utility for more wide-ranging species. Conversely, manual tracking systems allow for tracking fish (e.g., sharks) with longer migratory paths, but they are labor-intensive and often cost-prohibitive. Thus, the development of mobile tracking systems that can provide high positioning accuracy while simultaneously sampling environmental conditions would provide an essential tool in understanding how changes in environmental conditions influence movements of highly mobile fish. Sharks are of particular importance as they are considered apex predators and are important in shaping populations and communities lower in the food chain (Myers et al., 2007).

Proposed here is a prototype autonomous underwater vehicle (AUV) -based system that enables autonomous tracking and following of tagged fish that can provide relatively high-resolution position information (tens of meters) over long periods of time (many hours) and over greater coastal areas. The system combines an OceanServer Iver2 AUV with a Lotek MAP RT stereo-hydrophone system that measures signal strength and bearing to commercially available acoustic fish tags. The system uses a particle filter to estimate fish positions in real time, as well as a heuristic-based control strategy that allows for improved state estimation while simultaneously driving the AUV toward the tagged fish, but not beyond a preset perimeter. This enables tracking without chasing the tagged fish.

Details of the shark state estimator have been recently presented in Forney et al. (2012), and they are expanded upon in this work. As opposed to Forney et al. (2012), this paper presents details of sensor modeling, shark motion models, and postmission results that demonstrate that improvements to shark state estimation can be accomplished with improved shark motion modeling. To the best of our knowledge, the experiments documented in this paper are the first ever autonomous tracking and following of a tagged shark.

The paper is organized as follows. Section 2 discusses related works and elaborates on existing research. Section 3 provides an overview of the AUV tracking system. Section 4 describes the state estimator and control scheme. Experiments are described in Section 5, with results to follow in Sections 6 and 7. Conclusions and future work are presented in Section 8.

2. BACKGROUND

While a wide variety of underwater tracking technologies exist, the limitations of positional accuracy, spatial coverage, degree of labor intensity, and operational costs have limited movement studies of large, highly mobile fish, such as sharks (Lowe and Goldman, 2001).

Fine-scale fish movements are typically quantified with an acoustic telemetry tracking system, generally comprised of two parts: a transmitter and a receiver. The transmitters, often referred to as "tags," can be implanted into or attached to a fish, and they are designed to emit an acoustic signal between 30 and 200 kHz, depending on the size of the animal and the environmental conditions. The transmitter can produce a uniquely identifiable ultrasonic pulse or pulse train at fixed or varied intervals that enable the fish to be localized using an array of omnidirectional underwater receivers or a mobile shipborne receiver and directional hydrophone see, e.g., [Espinoza et al. (2011) Grothues and Dobarro (2009), and Lowe and Bray (2006)]. The distance from which a fish can be tracked is limited by the power output of the transmitter, but it typically varies between 50 and 1,000 m. More sophisticated tags can also transmit sensor information (e.g., depth, temperature, acceleration vectors) via their acoustic signal, which then have to be decoded by the receiver.

The receivers, usually one or more hydrophones, contain most of the power of the system and are responsible for decoding the tag's signal. Static underwater receiver arrays allow for a fish's position to be derived by triangulation or trilateration of the transmitter emission using the time of arrival of the transmitter pulse to neighboring receivers. These techniques allow for quantification of environmental parameters in addition to movements of multiple fish; however, if the tagged fish exhibit scopes of movement larger than the array, the fish cannot be tracked and positional accuracy decreases as the fish near the perimeter of the array (Espinoza et al., 2011). For example, the migratory movements of fish tagged in estuaries along the western Atlantic have been monitored using arrays in locations such as Maine and Virginia and also between estuaries in the eastern Pacific (Espinoza et al., 2011; Farrugia et al., 2011; Grothues and Dobarro, 2009). The alternative approach is to actively follow a tagged fish from a vessel using a directional hydrophone and shipborne receiver to determine bearing and distance based on signal strength and direction (Bellquist et al., 2008; Lowe et al., 2003; Mason and Lowe, 2010; Topping et al., 2005). This method can be extremely labor-intensive and cost-prohibitive, especially for large, highly mobile species.

Related to this research is the many years of investigation and development of target motion analysis (TMA). In TMA, sea vessels use passive sonar to obtain bearing-to-target information. A time series of such bearing measurements, combined with the known location of the sea vessel, allows for estimation of the target's range, course, and speed (Cunningham and Thomas, 2005; Kronhamn, 1998). Unlike typical TMA problems, the work presented here addresses the problem of sign ambiguity in the bearing-to-target measurement.

Using robots to track and follow moving objects in itself is not novel. For example, there have been several projects developed to accomplish dynamic tracking systems based on vision. In Schulz et al. (2001), joint probabilistic data association filters are used in conjunction with particle filters in order to track multiple humans inside a building, and they are able to successfully and reliably keep track of multiple persons (Schulz et al., 2001). The joint probabilistic data association filter is an algorithm that improves the separation and individual identification of data when tracking multiple objects. This particular study compares the success of Kalman filters to the success of particle filters when tracking a moving being. An additional study (Schulz et al., 2003) also used particle filters and joint probabilistic data association filters to determine the location of people in an office-type environment. Similarly, in Treptow and Zell (2004), visual data are acquired by the robot in order to determine its desired movement path. That particular study focused on soccer-playing robots that need to track the location of a soccer ball in order to determine their next move. In Schulz et al. (2001), a particle filter algorithm is used to predict the location of the ball.

When in close proximity, underwater robots have been shown to track moving objects using onboard vision systems (Georgiades et al., 2004). In Zhou and Clark (2006), a vision system was developed to conduct tracking of fish with a remotely operated vehicle (ROV); however, it was not implemented for autonomous tracking experiments. In Rife and Rock (2003), a vision system was used to successfully track and follow a jellyfish with an ROV.

The work in Goudey et al. (1998) represents some of the first work in attempting to equip a waterborne vehicle with the ability to autonomously track a tagged fish. A prototype surface vehicle was equipped with a single Vemco hydrophone receiver capable of detecting fish tag signals. The system demonstrated successful system integration and the ability to measure the bearing to the tag by rotating a directional hydrophone, although fish position was estimated to be that of the vehicle. As pointed out by Goudey et al. (1998), their system could benefit from multiple hydrophones that yeild measurements of the bearing to tag angle.

AUVs have been equipped with acoustic receivers to passively record acoustic tag signals. In Grothues et al. (2008), an AUV was used to gather data from two tagged Atlantic sturgeon in the Hudson River. This study demonstrated that AUV's are highly useful in gathering data on a tagged fish. Grothues et al. (2010) validated the use of hydrophones mounted on a moving AUV to track a tagged marine animal.

In Grothues et al. (2010), the necessity for en route decision making in AUVs was identified as a problem that needed to be addressed. AUVs have been programmed to follow a designated GPS waypoint path, recording information as they travel. Prior to this project, there had yet to be an AUV that could continually follow a single acoustic tag on a specific animal (shark) and make position estimates in order to follow the changing position of the animal. Real-time localization of the shark is necessary to track and follow it as it moves, as well as record its movement patterns. A major part of this real-time localization is the sensor fusion required for such state estimation. The AUV was equipped with a stereo-hydrophone receiver system which provided differential time of arrival data necessary for state estimation. This paper presents a particle-filter-based method for combining measurements from the stereo-hydrophone receiver over time, enabling real-time planar estimation of the shark state.

3. SYSTEM OVERVIEW

The proposed AUV tracking system is comprised of an Oceanserver IVER2 AUV (Figure 1) integrated with a Lotek MAP600RT stereo-hydrophone and receiver. The AUV is a torpedo-shaped robot actuated with two rear fins to control pitch, two rear fins to control yaw, and a rear propeller to provide locomotion. As shown in Figure 2, U represents the control vector sent to each of these five motors. The AUV's antenna mast has a built-in GPS receiver providing longitude and latitude measurements at a rate of 1 Hz when the AUV is at the surface. A kinematic model is used for position state estimation when below the surface. These position measurements are represented here as Z_{GPS}. The AUV also has a three-axis digital compass, which provides a yaw measurement Z_θ.

The AUV has two processors, the primary one of which runs waypoint tracking missions, monitors the status of the robot's actuators, and enables sensor and actuator communications. The secondary processor is designated for external programs, and it is where the acoustic receiver software, estimator, and controller are run. The Lotek receiver software produces measurements of the bearing to the tag z_α and signal strength z_{ss}, and it passes these measurements to the estimator. The estimator processes the inputs and then outputs the estimated shark state X_{shark}, which it sends to the controller. The controller takes X_{shark} as an input and uses this to make decisions about the movement of the AUV relative to the estimated shark position.

The stereo-hydrophones, acoustic receiver, and receiver software are part of the Lotek MAP RT-A Hydrophone sensor system. The hydrophone system is designed to listen for frequencies of 76 kHz, the same frequency of signals emitted by the Lotek brand tags. The tags transmit encoded analog signals that allow them to be identified uniquely on the same frequency. This permits tracking of a single individual within a group of many tagged individuals. Additionally, tag signals can be modulated to transmit depth information, enabling accurate depth estimation if required. An external frame was created in order to hold the stereo-hydrophones in place. The Lotek MAP RT-A system was designed to have the hydrophones set 2.4 m apart, and at least 1 m below the

Figure 1. The OceanServer Iver2 AUV equipped with a test stereo-hydrophone acoustic receiver system. Two protoype configurations are shown. In (a), a carbon fiber frame is used to attach the hydrophones. In (b), a pvc tube frame is used.

surface of the water. The hydrophone cables are internally connected and fed through sealed holes in the tail end of the hull of the AUV.

4. STATE ESTIMATION AND CONTROL

The proposed system uses an estimation method in which the AUV alters its control signals to increase information gain. As described below, the estimation method aids in reducing the effects of sign ambiguity in the bearing measurements.

4.1. Shark State Estimation

The estimation problem is depicted in Figure 3. In this figure a top down view of this system is shown with hydrophones h_1 and h_2 positioned just ahead of the AUV nose and just behind the AUV tail, respectively. X_{AUV} represents the position and yaw of the AUV with respect to an inertial coordinate frame and is determined by OceanServer's proprietary software. The estimator uses X_{AUV} and Z_t as inputs to estimate the shark state X_{shark} comprised of the two-dimensional (2D) planar position $[x_{\text{shark}}\ y_{\text{shark}}]$, heading angle θ_{shark}, forward velocity v_{shark}, and rotational velocity w_{shark} at each time step t. More precisely, for $t \in [0, t_{\max}]$,

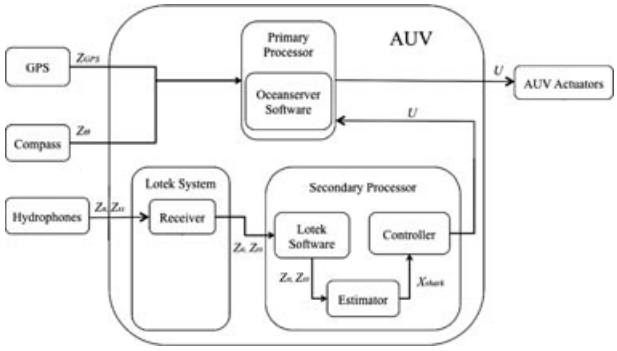

Figure 2. Flow of control variables through the AUV tracking system, from sensors to actuators.

Given that

$$X_{\text{AUV},t} = [x_{\text{AUV}}\ y_{\text{AUV}}\ \theta_{\text{AUV}}\ \dot{x}_{\text{AUV}}\ \dot{y}_{\text{AUV}}\ \dot{\theta}_{\text{AUV}}]_t, \tag{1}$$

$$Z_t = [z_{\text{ss}}\ z_\alpha]_t, \tag{2}$$

determine

$$X_{\text{SHARK},t} = [x_{\text{shark}}\ y_{\text{shark}}\ \theta_{\text{shark}}\ v_{\text{shark}}\ w_{\text{shark}}]_t. \tag{3}$$

Challenges associated with the stereo-hydrophone system include its limited range ($L \approx 100$ m), its low resolution ($= \pi/9$ rad), and the ambiguity of the sign of the bearing angle. This ambiguity is illustrated in Figure 3, where the AUV cannot determine if a single bearing measurement z_α corresponds to angle $+\alpha$ or $-\alpha$. X'_{shark} represents the other possible location of state based on the ambiguous sensor reading. The limited range was determined through experiments as the distance at which the signals were consistently lost. The signal strength value z_{ss} was not used in real-time estimation due to the inconsistencies seen in the range of the tags.

There exist a variety of filtering methods which are commonly used in robotics for state estimation including applications in localization and mapping (Thrun et al., 2005). These techniques are largely based on Kalman

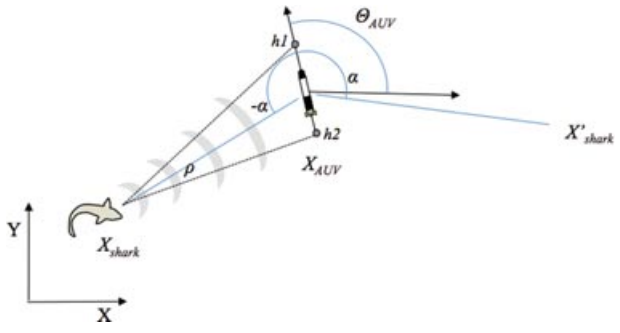

Figure 3. Top down view of the sample measurement.

filter (KF) or Monte Carlo (MC) methods. One such method, particle filter (PF) estimation, is heavily based on the MC localization algorithm (Thrun et al., 2001). A particle filter state estimator approximates a belief state using a set of particles (Thrun et al., 2005). Each particle represents a single randomized representation of state and has an associated weight that represents the likelihood it is the actual state. Together, the set of particles creates a multiple hypothesis sample set. In this work, the particle filter's ability to accommodate multiple hypotheses of the state is leveraged to deal with a stereo hydrophone system that cannot determine the sign of the relative angle to a detected fish tag.

The PF used to estimate the state of the shark uses a set of P particles, each with a state defined in Eq. (3). Each particle represents a single estimate of the shark state, with a position, orientation, velocity, and weight. Initially, each particle is randomly assigned a position, orientation, and velocity by selecting from a uniform random distribution. Planar positions (x, y) are randomly selected from a $2L$ meter by $2L$ meter square area with the initial location of the AUV as the center of the distribution. Here, L is the range of the acoustic receiver system.

After being initialized, particles are updated with the PF algorithm that is called at each iteration of the AUV's control loop. The algorithm has two main steps, a *prediction* step and a *correction* step. The prediction step predicts the shark state of every particle. If a new valid signal from the shark tag is received, the likelihood or weight of all particles is calculated and the correction step will be called to resample the particle distribution. At the end of these two steps, the shark state estimate can be calculated as the state estimate of highest weight or as the weighted average for position, orientation, and velocity of all P particles.

Algorithm 1. PF_Shark_State_Estimator($\{X^p\}$, X_{AUV}, z_α, z_{ss})

1: *//Prediction*
2: **for all** p particles **do**
3: $X^p_{\text{shark},t} \leftarrow \text{Motion\_Model}(X^p_{\text{shark},t-1})$
4: **if** z_α is valid **then**
5: $\alpha^p_{\text{exp}} \leftarrow \text{atan2}(y^p_{\text{shark}} - y_{\text{AUV}}, x^p_{\text{shark}} - x_{\text{AUV}}) - \theta_{\text{AUV}}$
6: $\alpha^p_{\text{exp}} \leftarrow g_\alpha(\alpha^p_{\text{exp}})$
7: $\text{ss}^p_{\text{exp}} \leftarrow g_{\text{ss}}(dist^p_{\text{exp}})$
8: $w^p \leftarrow h(z_\alpha, \alpha^p_{\text{exp}}, z_{\text{ss}}, \text{ss}^p_{\text{exp}})$
9: **end if**
10: **end for**
11:
12: *//Correction*
13: **if** α is valid **then**
14: $\{X^p\}_{\text{temp}} \leftarrow \{X^p\}$ for all p
15: **for all** p particles **do**
16: $X^p \leftarrow RandParticle(\{X^p\}_{\text{temp}})$
17: **end for**
18: **end if**

4.1.1. Prediction Step

At every time step, each of the P particles in the set $\{X^p\}$ is propagated forward according to a first-order motion model (Line 3 of Alg. 1). The motion model is a function of the previous particle position $(x^p_{\text{shark}}, y^p_{\text{shark}})$, orientation θ^p_{shark}, velocity v^p_{shark}, and the uncertainty associated with these values, specifically the standard deviations σ_θ and σ_v.

Several motion models were considered for this prediction step, most of which are based on mathematical models that attempt to describe the motion tendencies of individual animals that have been tracked in previous tagging and tracking experiments. For example, diffusion models have been applied to a variety of species to represent dispersal of fish populations (Hilborn, 1990, Johnson et al., 1992, Skalski and Gilliam, 2000). At the individual level, diffusion modeling can be incorporated into an individual's movements using a particle-based approach that models movements as a random walk [see e.g., Bailey and Thompson (2006)]. Several types of random walks have been considered, including Brownian motion and Levy flights (Sims et al., 2011) as well as mixtures (Morales et al., 2004). For example, the Levy flight foraging hypothesis, in which optimal foraging for predators is accomplished with Levy flights when prey is sparse, was confirmed by Humphries et al. (2010) for particular shark species for which extensive tracking data existed. The uncertainty of such movement models was incorporated into a state space formulation in Jonsen et al. (2005), allowing a comparison between different movement behavior models via error covariance.

Other particle models assume an individual follows simple kinematic equations that are affected by the state of its local neighbors (Hensor et al., 2005; Huse et al., 2002; Katz et al., 2011). For example, in Hensor et al. (2005), an individual's motion is a function of its repulsion, alignment, and attraction to other individuals. From these interactions, there can emerge general trends in the movement of the population. This is often seen in shoaling, schooling, and aggregating species. This grouping behavior and the predictability of the movements of the group can have great consequences on the dispersal of bioaccumulated contaminants, overharvesting, and ultimately ecosystem health.

The particular motion models investigated here include a *MomentumRandomWalk*, *BrownianRandomWalk*, and a *LevyFlight*. For the *MomentumRandomWalk* (Alg. 2), the velocity, v^p_{shark}, is randomly sampled from a Gaussian distribution with a mean equal to the previous particle velocity and standard deviation equal to the expected change in shark velocity. The step direction, θ^p, is randomly sampled from a Guassian distribution with a mean equal to the previous particle yaw θ^p_{shark} and standard deviation equal to the expected change in yaw.

Algorithm 2. Motion_Model_MomentumRandomWalk($X^p_{\text{shark},t}$)

1: $//MomentumRandomWalk$
2: $v^p_{\text{shark}} \leftarrow NormalRandom(v^p_{\text{shark}}, \sigma_v)$
3: $\theta^p_{\text{shark}} \leftarrow NormalRandom(\theta^p_{\text{shark}}, \sigma_\theta)$
4: $x^p_{\text{shark}} \leftarrow x^p_{\text{shark}} + v^p_{\text{shark}} \cos(\theta^p_{\text{shark}})\Delta t$
5: $y^p_{\text{shark}} \leftarrow y^p_{\text{shark}} + v^p_{\text{shark}} \sin(\theta^p_{\text{shark}})\Delta t$

For the $BrownianRandomWalk$ (Alg. 3), the velocity, v^p_{shark}, is randomly sampled from a uniform random distribution between 0 and $v_{\max}$, where $v_{\max}$ is a maximum velocity. The step direction, θ^p, is randomly sampled from a uniform random distribution between $-\pi$ and π.

Algorithm 3. Motion_Model_BrownianRandomWalk($X^p_{\text{shark},t}$)

1: $//BrownianRandomWalk$
2: $v^p_{\text{shark}} \leftarrow UniformRandom(0, v_{\max})$
3: $\theta^p_{\text{shark}} \leftarrow UniformRandom(-\pi, \pi)$
4: $x^p_{\text{shark}} \leftarrow x^p_{\text{shark}} + v^p_{\text{shark}} \cos(\theta^p_{\text{shark}})\Delta t$
5: $y^p_{\text{shark}} \leftarrow y^p_{\text{shark}} + v^p_{\text{shark}} \sin(\theta^p_{\text{shark}})\Delta t$

For the $LévyFlight$ motion model (Alg. 4), the step direction is also randomly sampled from a uniform random distribution from $-\pi$ to π. However, the step length is randomly sampled from the heavy tailed probability density function Pr(l), shown in Eq. (4).

$$\Pr(l) = \frac{\gamma}{\pi[l^2 + \gamma^2]}. \tag{4}$$

In this distribution, the distance l is likely to be short but does have a minimum likelihood of larger l values. This typically results in a random motion involving many small steps followed by a large step. Tuning studies (Viswanathan et al., 1999) on different species have suggested that the distribution decays according to $\Pr(l) = l^{-2}$. To achieve similar behavior, γ is set to achieve similar exponential decay while considering the size of the time step Δt.

Algorithm 4. Motion_Model_LévyFlight($X^p_{\text{shark},t}$)

1: $//LévyFlight$
2: $l^p_{\text{rand}} \leftarrow LévyDistance(\Delta t)$
3: $\theta^p_{\text{shark}} \leftarrow UniformRandom(-\pi, \pi)$
4: $x^p_{\text{shark}} \leftarrow x^p_{\text{shark}} + l^p_{\text{rand}} \cos(\theta^p_{\text{shark}})$
5: $y^p_{\text{shark}} \leftarrow y^p_{\text{shark}} + l^p_{\text{rand}} \sin(\theta^p_{\text{shark}})$

4.1.2. Weight Calculation

Particle weights are only calculated (Alg. 1, lines 5–8) when a "valid" tag detection is received, i.e., when both hydrophones detect a signal from the tag to enable calculation of the bearing. This actual bearing measurement z_α is compared with the expected bearing measurement for each particle α^p_{exp} to determine the weight of the particle. Ideally, the closer the match between these two bearings, the higher the weight.

When a new bearing measurement is calculated by the Lotek MAPHost software, the bearing value is written to a text file accessible to the estimator. The coordinate system and units of this measurement are not conventional in that they are integer values that span from −9 to 9, which are roughly mapped to a range of -90° to $+90^\circ$. A value of 0 indicates the tag is in the direction perpendicular to the baseline separating the hydrophones. Figure 4(a) illustrates a third-order polynomial mapping between measured bearing angle in degrees to units exported by the Lotek MapHost software.

To create the mapping function between these two units, a large number of ocean experiments were conducted in which bearing angle was varied from -90° to $+90^\circ$ (in increments of 45°) and the range between the tag and the AUV was varied from 25 to 200 m (in increments of 25 m). Using data from such experiments, a least-squares best fit was used to generate a model of the relationship between units. Equation (5) provides an example of a third-order model generated for the data in Figure 4(a), that converts the bearing units from degrees to Lotek MAPHost software units.

$$g_\alpha\left(\alpha^p_{\text{exp}}\right) = -1 \times 10^{-6}\left(\alpha^p_{\text{exp}}\right)^3 + 2 \times 10^{-5}\left(\alpha^p_{\text{exp}}\right)^2 + 0.0947\alpha^p_{\text{exp}} - 0.2757. \tag{5}$$

The function $g_\alpha()$ in Eq. (5) is used to convert the expected bearing to the shark α^p_{exp} for any particle p from degrees to Lotek MAPHost software units. Note that it is straightforward to calculate the expected bearing in degrees using the shark state of the particle X^p_{shark} and the AUV state X_{AUV}. This calculation followed by the conversion is shown on lines 5 and 6 of Alg. 1.

The particle can be assigned a weight on line 8 of Alg. 1 through the following Gaussian weighting function:

$$h_\alpha(z_\alpha, \alpha^p_{\text{exp}}) = 0.001 + \frac{1}{\sqrt{2\pi}\sigma_\alpha} e^{\frac{-(\alpha^p_{\text{exp}} - z_\alpha)^2}{2\sigma^2_\alpha}}. \tag{6}$$

The weight has a minimum value of 0.001 and is given a higher value when the particle's expected angle, α^p_{exp}, is closer to the measured angle, z_α. As the angle difference decreases, a higher weight value is assigned. The standard deviation σ_α of the Gaussian function was determined using the same experiments described above. The results are shown in Table I.

Weight calculations may also consider the signal strength measurements as a sensor value. While work in Forney et al. (2012) that used the PF in real time did not

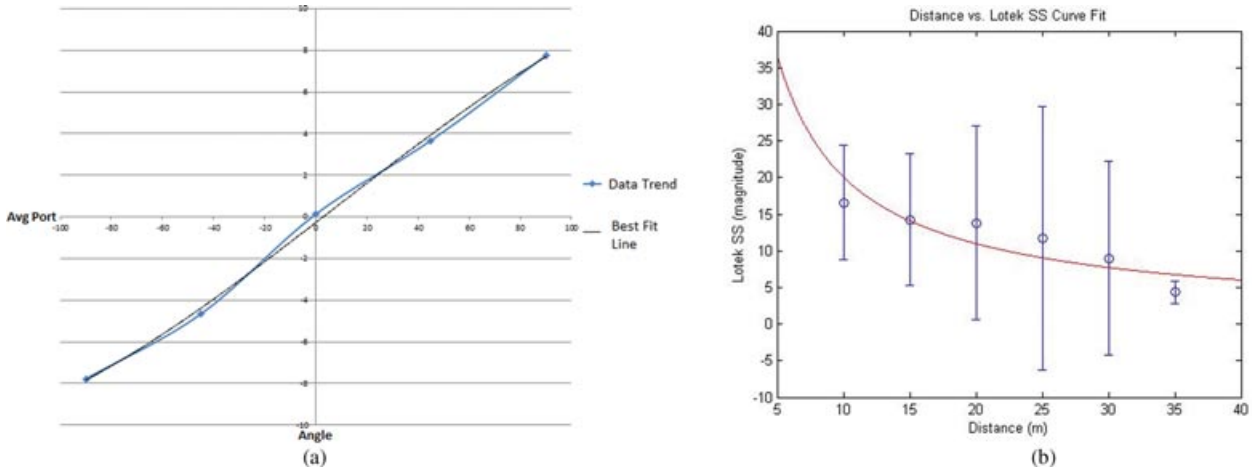

Figure 4. Mapping hydrophone measurements. In (a), the polynomial function representing the mapping from bearing measurements in degrees to Lotek MAPHost software units. In (b), a polynomial function representing the mapping from distance (m) to signal strength in Lotek MAPHost software units.

Table I. Filter parameter values.

Parameter	Value
σ_v	0.3 m per second
σ_θ	$\pi/2$ radians
σ_α	1.0 lotek angle units
σ_{ss}	15 lotek signal strength units

incorporate the signal strength value into the state estimation, it can be shown to provide a more accurate shark state estimation. A 1,500-s data set with measured distances (using GPS) and Lotek signal strengths was used to create a mapping between signal strength and distance. The data were split into bins of 5 m. The Lotek hydrophone signal strength in each of the bins is averaged and displayed in Figure 4(b) with error bars indicating the standard deviation. A curve fit was found based on the model that the signal strength "ss" versus distance "dist" relationship is linear on a logarithmic scale. The relationship is given by Eq. (7) for constants a and b:

$$\log_{10}(\text{ss}) = b + a * \log_{10}(\text{dist}). \tag{7}$$

Given a and b, the expression for ss is given by

$$g_{\text{ss}}(\text{dist}) = 10^b \times \text{dist}^a. \tag{8}$$

The resulting fit from experimental data produced values $a = -0.871$ and $b = 2.18$ as plotted in Figure 4b. Equation (8) can be used to determine ss^p_{exp} given an expected distance $\text{dist}^p_{\text{exp}}$. σ_{ss} is estimated from the standard deviations of the bins. The following Gaussian weighting function can then be used to weight distance in the particle filter:

$$h_{\text{ss}}(z_{\text{ss}}, ss^p_{\text{exp}}) = 0.001 + \frac{1}{\sqrt{2\pi}\sigma_{\text{ss}}} e^{\frac{-(\text{ss}^p_{\text{exp}} - z_{\text{ss}})^2}{2\sigma^2_{\text{ss}}}}. \tag{9}$$

The weight has a minimum value of 0.001 and is given a higher value when the particle's expected signal strength, ss_{exp} is closer to the measured signal strength z_{ss}. The standard deviation σ_{ss} of the Gaussian function was determined from past experiments. Finally, a proposed modified weighting function h_{mod} for a particle filter including bearing and sensor strength measurements is given by

$$h_{\text{mod}} = 0.001 + \frac{1}{\sqrt{2\pi}\text{ss}^p_{\text{exp}}} e^{\frac{-(\text{ss}^p_{\text{exp}} - z_{\text{ss}})^2}{2\sigma^2_{\text{ss}}}} \times \frac{1}{\sqrt{2\pi}\alpha^p_{\text{exp}}} e^{\frac{-(\alpha^p_{\text{exp}} - z_\alpha)^2}{2\sigma^2_\alpha}}. \tag{10}$$

4.1.3. Correction Step

Once weights are calculated using either of h_α, h_{ss} or h_{mod}, the particle population is randomly resampled to produce a set that has a higher proportion of particles with higher weights. The resampling is shown in Alg. (1), lines 13–18. A copy of the propagated particle set is saved in $\{X^p\}_{\text{temp}}$. Then, each particle state is repopulated by randomly selecting from $\{X^p\}_{\text{temp}}$ using the function $RandParticle()$. This function selects a particle at random, with a likelihood of selection proportional to the particle's normalized weight.

4.2. Control for Improved Estimation

To minimize the distance between the AUV and the shark, while trying to improve the shark state estimation, a

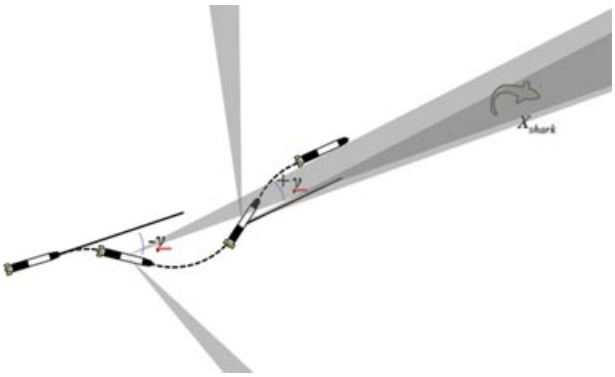

Figure 5. The control strategy: The AUV is stepped through a series of three desired headings to track. The sensor footprints after the first and second headings tracked are shown in gray.

repeated three-step controller was used in which the desired heading was changed at each step. To track each desired heading, a simple P controller was used (notably only stable assuming linear kinematics). Regardless, the heading error, $(\theta_{\text{des}} - \theta)$, has been shown to decay to zero for all real-time experiments. This control loop iterates at 1.0 Hz (i.e., time step size = 1 s), as limited by the communication with the Iver2's proprietary control software that handles all real-time actuation.

At the start of step 0 of the three-step controller, the estimated bearing to the shark β_0 is calcuated using the PF's shark state position estimate. Despite having intermittent Lotek measurements with possible errors, the PF fuses the measurements over time to produce an updated state estimate of highest likelihood (Thrun et al., 2005) at every iteration of the control loop. The desired heading θ_{des} is set relative to the same value of β_0 for each step 0, 1, and 2,

$$\theta_{\text{des},t} = \beta_0 + \gamma_t, \tag{11}$$

where

$$\gamma_t = \begin{Bmatrix} \frac{\pi}{4} & if & step = 0 \\ -\frac{\pi}{4} & else\ if & step = 1 \\ 0 & else\ if & step = 2 \end{Bmatrix}. \tag{12}$$

The controller increments the step variable by 1 once $|\theta_{\text{des},t} - \theta_t| < \tau$, where τ is a threshold representing tolerence on a heading tracking. The three steps are depicted in Figure 5, where the sensor footprints at the end of step 0 and step 1 are shown. This depiction highlights the advantage of changing the sensor's vantage point in that only particles residing in the overlap of these two footprints will obtain high weights during both sensor readings and have a greater likelihood of surviving resampling. Because of this approach, the negative effects of the sign ambiguity in the bearing measurements are reduced.

5. EXPERIMENTS

5.1. Avila Beach Pier Experiments

A series of validation experiments were performed at the Cal Poly Center for Coastal Marine Science (CCMS) (Figure 6a). The facility is located at the end of a large pier in Avila Beach, CA. A lower landing dock allows easy deployments of the AUV. Water depths are on the order of 8 m and the bay is relatively well protected from high surf and waves.

The experiments at the CCMS included sensor characterization (e.g., determine σ_α), AUV tracking of a stationary tag, and AUV tracking of a moving tag. During stationary and moving tag experiments, the AUV's start position relative to the tag was varied to ensure tracking could be performed from every direction. AUV start positions were also varied according to initial distance from the tag (i.e., 20, 50, 75, and 100 m). For moving tag experiments, the tag was attached to a second Iver2 AUV (AUV2). During these experiments, the tag was fixed 2.0 m below the surface, and the water depth was 10.0 m. AUV2's GPS receiver measurements were recorded to provide measurements of the tag's location as a function of time. Once the AUV was deployed for these experiments, it would autonomously track the tag's position estimates produced by the PF.

5.2. Port of Los Angeles Experiments

The experiments from CCMS were repeated in SeaPlane Lagoon, Port of Los Angeles, CA, to verify the accuracy and functionality in a new environment (see Figure 6b). The lagoon varies in depth from 0.0 to approximately 2.0 m. There is a high density of eel grass growth in some areas that can be problematic both for AUV navigation and attenuation of acoustic signals.

In addition to the same validation experiments conducted at CCMS, a 1-m-long leopard shark (*Triakis semifasciata*) was caught in the lagoon, externally fitted with an acoustic transmitter, and tracked (Lotek MM Series, 76 kHz freq, 2 s, and 5 s ping rate). This type of tag and attachment method are standard use for tagging large marine fishes. Once the tagged shark was released, the AUV was deployed to track and follow it.

6. REAL-TIME OCEAN TRACKING RESULTS

To validate the system and evaluate performance, the following metrics were used: shark state estimation error, shark state estimation error variance, and distance between the AUV and the shark position as a function of time. These metrics were applied both to real-time experiments as well as in off-line state estimation experiments using measurements logged during the real-time experiments.

Figure 6. Field sites used for system validation: In (a), a top down view of the Cal Poly Center for Coastal Marine Science (CCMS) is shown. In (b), Sea Plane lagoon in the Port of LA, CA is shown.

6.1. Stationary Tag Tracking Results

For stationary tag tracking experiments, the lower state estimation errors are expected, and there is an expectation that the distance between the AUV and the tag will be driven to a small bounded error over time. An example of a stationary tag experiment is shown in Figure 7. The position estimation error drops quickly to 10 m and stays relatively constant while the AUV continues its course toward the tag. This reduces the distance between the tag and the AUV until the 360th second. At this point, the AUV continues its control sequence to track $\pi/4$ radians left of the direct line to the target, which at that close distance moves the AUV away from the target. However, once it completes the control sequence it continues on toward the estimated tag

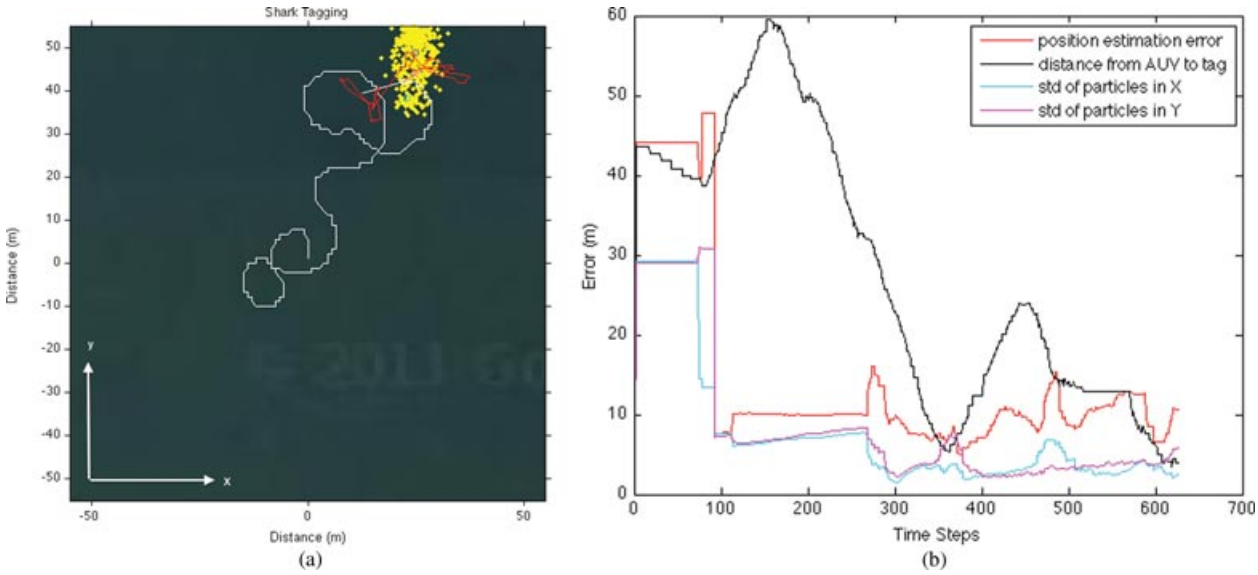

Figure 7. Tracking a stationary tag: In (a), the path of an AUV (white) as it autonomously navigates toward a stationary tag (cyan). The red path indicates the path of the tag as estimated by the AUV. Particle locations at the last time step are shown in yellow. In (b), error (m), distance to the shark, and standard deviation (m) of the position estimate are plotted for the same experiment.

position. The standard deviation of the particles in both directions can also be seen to decrease over time, indicating the particles are clustering to a size on the same order of magnitude as the error.

Note that the control system used here drives the AUV toward the shark. However, the closer the AUVs are to the shark, the more likely the presence of the AUV will influence the behavior of the shark, making the more accurate positions useless from an ecological standpoint. To account for this, the AUV is programmed to remain motionless when it is within some predetermined distance of the shark to enable accurate shark localization without altering shark behavior.

6.2. Moving Tag Tracking Results

To demonstrate system performance with a moving target, results are presented from an experiment in which an acoustic tag was attached to a second Iver2 AUV. Figure 8(a) shows the paths for both the tracking vehicle (named AUV) and the tagged vehicle (named AUV2). AUV2 was manually driven within the lagoon, mimicking the relatively slow movement of a leopard shark. AUV autonomously tracked and followed AUV2 using the PF and controller described above. To note, the speed of AUV2 was bordering on the maximum speed that still allowed AUV1 to track and follow it.

The error and standard deviations can be seen in Figure 8(b). At t = 2,500 s, there is a significant increase in error. This corresponds with poor quality acoustic measurements we observed as the AUVs crossed an area with a high density of eel grass. This can be observed as the darker coloring in the center of Figure 8(a).

The signal rate, i.e., the frequency of usable measurements, is also plotted. As expected, as the signal rate decreases, standard deviations and error increase. Though the tag emits a signal every 2 s, many of the signals are unusable (only one hydrophone picked up the signal) or are not picked up at all. For example, the maximal signal rate for the stationary experiment was 30 signals/min, and the highest signal rate seen was just over 25 signals/min. Unfortunately, due to environmental factors and the short range of the tag signal, rates as low as 3 signals/min were seen.

6.3. Shark Tracking Results

On August 8, 2011, a leopard shark was tagged and released in the early afternoon. It initially moved away from the location of capture to a deeper portion of the lagoon before returning in the late afternoon. The AUV was deployed to conduct autonomous tracking, but it was relatively unsuccessful since the shark moved to a very shallow beach area (≈0.40 m depth), which is a common behavior of leopard sharks during this time of year. The AUV continuously attempted to drive itself into this shallow area to follow the shark, only to dig the frame and hydrophones into the sandy bottom.

On August 9 and 10 of 2011, the AUV was deployed with a shorter hydrophone support frame, and the tagged leopard shark was successfully tracked by the AUV for several hours with little interruption while it moved in a deeper portion of the lagoon. The experiments were stopped only a few times for the following reasons: 1) the batteries in the laptops used by researchers to monitor the experiments were low, 2) the AUV batteries were low, and 3) the AUVs had been programmed to halt tracking operations after 45 min to reduce the risk of loss. In the future, an

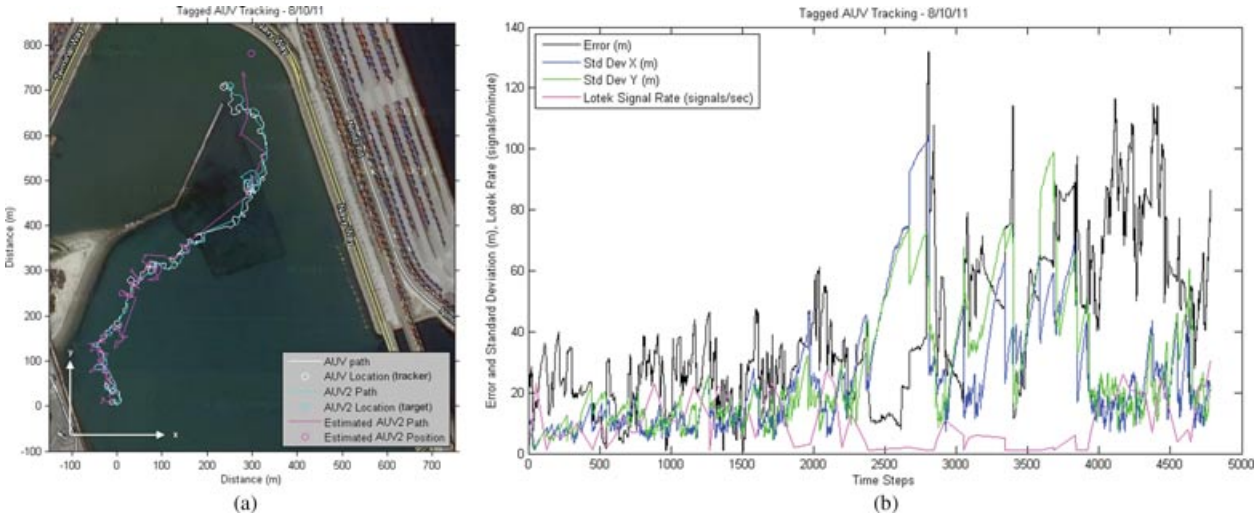

Figure 8. Tracking a tagged AUV: The trajectories of the tracking AUV, the tagged AUV2, and AUV2 as estimated by AUV are shown.

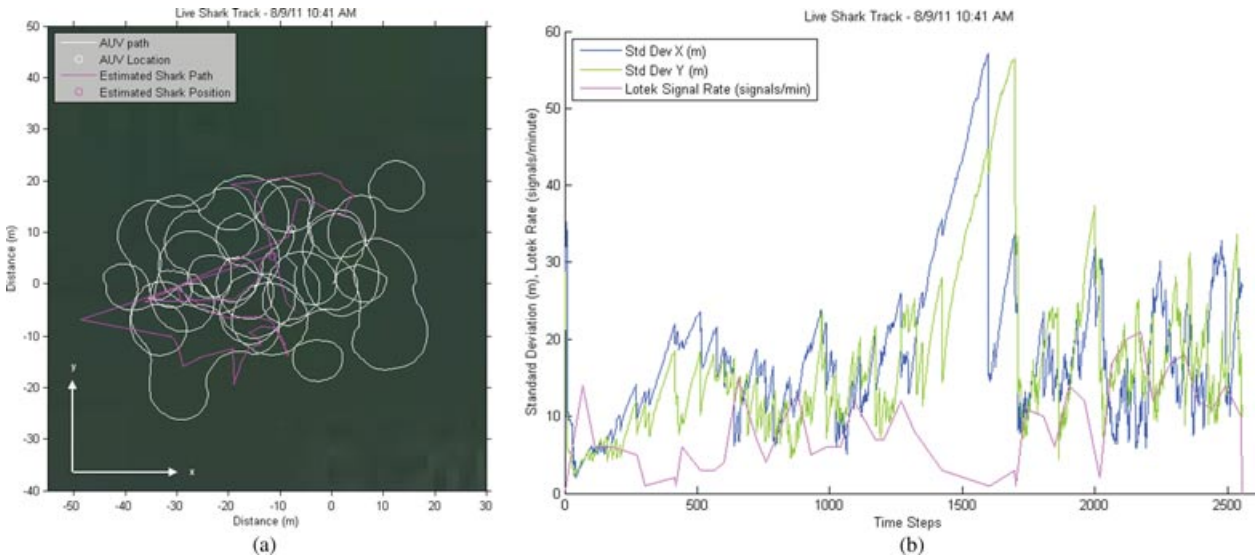

Figure 9. Tracking a tagged shark: In (a), the trajectories of the tracking AUV and the estimated position of the tagged shark are shown. In (b), the standard deviation (m) of the position estimate and the signal rate (signals/min) of the same experiment are shown.

automobile battery and inverter could be used to remedy issue 1).

The AUV and estimated shark paths from a 48-min-long tracking experiment are shown in Figure 9(a). Figure 9(b) shows the corresponding standard deviations of the particle set as well as the signal rate from the acoustic tag. While no estimation accuracy was obtained, these experiments demonstrated the ability for long-term autonomous AUV tracking and following of a live shark, while not chasing it. Table II summarizes the results, with a notable maximum tracking time of 1.67 h.

Table IV and Table V show statistics about missions that were performed. The misson length and area covered give an indication of the duration and difficulty of the experiments. The tables demonstrate that stationary tracking has better results due to the fact that signal rate declines in the moving experiments with the introduction of external factors. This is depicted in Figure 8(b) by the error spike at time step 2,500 where the received signal rate drops to close to zero. The standard deviations are a measure of error uncertainty. The proportion of time at which the error was less than the standard deviation of the particle spread is shown in Table II for the two AUV experiments. Errors were less than the standard deviations 42.12% of the time.

Table II. Comparing error with standard deviation.

Comparison	Proportion of smaller error (%)
$e_x < \sigma_{\text{avg}X}$	36
$e_y < \sigma_{\text{avg}Y}$	42
$e_x < \sigma_X$	22
$e_y < \sigma_Y$	26
$e < \sigma$	42

While only one shark was tagged, it was tracked and followed for several hours at a time over a two-day period. A greater number of longer duration experiments with varying conditions are planned to further validate the robustness of the system.

7. OFFLINE RESULTS

Using the first 1,500 s of the two AUV experimental datasets, several classes of particle filters were investigated and compared for potential improvement over the PF used during the real-time tracking experiments:

1. **Standard PF** used for real-time estimation during the tracking experiments. The prediction step used the *MomentumRandomWalk* model and the correction step used only bearing measurements to weight particles.
2. **Acoustic SS PF** The prediction step used the *MomentumRandomWalk* model and the correction step used bearing and signal strength measurements to weight particles.
3. **Brownian Only PF** The prediction step used the *BrownianRandomWalk* model and the correction step used only bearing measurements to weight particles.
4. **Lévy PF** The prediction step used the *LévyFlight* model and the correction step used only bearing measurements to weight particles.
5. **Combined Brownian PF** The prediction step used the *BrownianRandomWalk* model and the correction step used

Table III. Average error of particle filters for first 1,500 s (values given in meters).

Particle filter type	Mean	25th quartile	Median	75th quartile
Standard PF	24	23	24	24.4
Acoustic SS PF	21	21	21	22
Brownian only	19	19	19	19
Lévy $\gamma = 1e-2$	32	24	28	32
Lévy $\gamma = 1e-1$	23	22	23	24
Lévy $\gamma = 1e0$	39	39	39	40
Combined Brownian	17	17	17	18
Combined Lévy $\gamma = 1e-3$	93	78	93	107
Combined Lévy $\gamma = 1e-2$	22	20	21	24
Combined Lévy $\gamma = 1e-1$	22	22	23	23
Combined Lévy $\gamma = 1e0$	28	27	28	28

Table IV. Mission data.

Mission name	Date	Time of day	Mission length (min)	Area covered (m^2)
sharkTrackA	8/9/11	10:41	48	14,025
sharkTrackB	8/9/11	12:07	37	3,150
sharkTrackC	8/9/11	14:42	41	9,720
sharkTrackD	8/9/11	15:33	1:41	7,280
auv2Track	8/10/11	11:19	1:38	27,7148
stationaryTrackA	8/7/11	16:19	4	2,408
stationaryTrackB	8/7/11	16:24	10	1,782
stationaryTrackC	8/7/11	20:47	10	2,376

Table V. Mission results.

Mission name	Avg error (m)	Min error (m)	Max error (m)	Min σ_x (m)	Max σ_x (m)	Min σ_y (m)	Max σ_y (m)
sharkTrackA	n/a	n/a	n/a	4.23	51.59	3.44	56.12
sharkTrackB	n/a	n/a	n/a	4.95	52.10	2.79	46.89
sharkTrackC	n/a	n/a	n/a	1.54	79.83	2.77	65.75
sharkTrackD	n/a	n/a	n/a	1.91	80.91	2.34	87.72
auv2Track	41.73	0.85	140.43	0.85	106.95	1.51	112.75
stationaryTrackA	7.01	0.25	15.46	2.61	13.43	3.17	12.00
stationaryTrackB	16.88	1.53	47.26	6.92	23.51	4.42	32.68
stationaryTrackC	21.70	3.13	47.54	4.21	29.10	3.49	31.05

bearing and signal strength measurements to weight particles.

6. **Combined Lévy PF** The prediction step used the *LévyFlight* model and the correction step used bearing and signal strength measurements to weight particles.

A total of 100 trials were run for each PF design and the error was averaged over each trial. The results are given in Table III.

The signal-strength based particle filter and Brownian motion model particle filter had an average error that was lower than that of the standard particle filter. The Lévy flight motion model particle filter demonstrated an average error approximately equal to or greater than that of the standard particle filter depending on the scaling parameter. The most effective particle filter combined the Brownian motion model for the prediction step and the signal strength sensor value in the correction step. It had the lowest average error of all the particle filters.

These results provide evidence that the usage of the signal strength can be an effective sensor value in the particle filter. Its inclusion in the standard particle filter and motion

model based particle filters improved performance. It also shows that alternative models of shark behavior, such as Brownian motion, could be effective in state estimation.

There may be an explanation for the relatively high error for Lévy flight based particle filters. Particle filters based upon specific behavioral models, such as a Lévy flight, would be expected to be most effective when tracking a living member of that species behaving in a normal manner. The data set consists of an AUV autonomously tracking a human-controlled AUV that was attempting to mimic a shark. It may be that a particle filter based upon a Lévy flight could be more effective when tracking living sharks in the field.

8. CONCLUSIONS AND FUTURE WORK

This work presented results from the first attempt to autonomously track and follow a shark using an autonomous underwater vehicle. Despite the current prototype hydrophone configuration having high drag, the ambiguity in bearing measurement sign, the high variance in signal strength measurements to distance mapping, and the low signal reception rate, the AUV was still able to follow a tagged leopard shark for several hours.

There is considerable work to be done to improve this system, including reducing the hydrophone frame profile and drag, incorporating multiple AUVs, demonstrating the use of signal strength measurements during real-time state estimation, and developing optimal control policies for active shark state estimation.

While the shark state estimation accuracy seems to be on par with current mobile tracking methods, i.e., via a human-driven surface vessel, future work will include a systematic comparison between methods. Specifically, similar tracking experiments (of a tagged shark) could be conducted while simultaneously employing one of the traditional manual tracking methods.

As part of future work, the controller will be extended to 3D motion by using the pitch control fins to incorporate undulations as part of the AUV path. That is, the AUV will be programmed to dive and surface at regular time intervals [as the authors have done in Clark et al. (2013)], to balance the trade-off between increasing AUV state estimation with surface-enabled GPS measurements upon increasing the frequency of variable depth-obtained ocean sampling measurements.

The system presented can also easily be extended to include the capability to enter a circular search pattern (of growing radius) when no tag signals have been detected for a certain amount of time. In moving toward tracking experiments of longer duration, researchers must address the issue of the limited battery life of the AUV, as well as ensuring maximum efficiency by minimizing the sensor configuration profile to reduce drag.

ACKNOWLEDGMENTS

This work would not have been accomplished without the help of Victoria Campo and Justin Knight, who aided in sensor calibrations. This material is based upon work supported by the National Science Foundation under Grant No. 1245813.

REFERENCES

Bailey, H., & Thompson, P. (2006). Quantitative analysis of bottlenose dolphin movement patterns and their relationship with foraging. Journal of Animal Ecology, 75(2), 456–465.

Bellquist, L. F., Lowe, C., & Caselle, J. (2008). Fine-scale movement patterns, site fidelity, and habitat selection of ocean whitefish (caulolatilus princeps). Fisheries Research, 91, 325–335.

Clark, C., Hancke, K., Xydes, A., Hall, K., Schreiber, F., Klemme, J., Lehr, J., & Moline, M. (2013). Estimation of volumetric oxygen concentration in a marine environment with an autonomous underwater vehicle. Journal of Field Robotics, 30(1), 1–16.

Cunningham, A., & Thomas, B. (2005). Target motion analysis visualisation. In S.-H. Hong (Ed.), Asia Pacific Symposium on Information Visualisation (APVIS2005) (vol. 45, pp. 81–90), ACS.

Espinoza, M., Farrugia, T., Webber, D., Smith, F., & Lowe, C. (2011). Testing a new acoustic technique to quantify fine-scale, long-term fish movements. Fisheries Research, 108(2-3), 364–371.

Farrugia, T. J., Espinoza, M., & Lowe, C. (2011). Abundance, habitat use and movement patterns of the shovelnose guitarfish (rhinobatos productus) in a restored southern california estuary. Marine and Freshwater Research, 62(6), 648–657.

Forney, C., Manii, E., Farris, M., Moline, M. A., Lowe, C., & Clark, C. M. (2012). Tracking of a tagged leopard shark with an auv: Sensor calibration and state estimation. IEEE International Conference on Robotics and Automation, 5315–5321.

Georgiades, C., German, A., Hogue, A., Liu, H., Prahacs, C., Ripsman, A., Sim, R., Torres, L., Zhang, P., Buehler, M., et al. (2004). Aqua: An aquatic walking robot. In Intelligent Robots and Systems 2004 (IROS 2004), Proceedings of the 2004 IEEE/RSJ International Conference (vol 4, pp. 3525–3531), IEEE.

Goudey, C., Consi, T., Manley, J., Graham, M., Donovan, B., & Kiley, L. (1998). A robotic boat for autonomous fish tracking. Marine Technology Society Journal 32(1).

Grothues, T., & Dobarro, J. (2009). Fish telemetry and positioning from an autonomous underwater vehicle (auv). Instrumentation ViewPoint, 8, 78.

Grothues, T., Dobarro, J., & Eiler, J. (2010). Collecting, interpreting, and merging fish telemetry data from an AUV: Remote sensing from an already remote platform. Autonomous Underwater Vehicles (AUV), 2010 IEEE/OES (pp. 1–9).

Grothues, T., Dobarro, J., Ladd, J., Higgs, A., Niezgoda, G., & Miller, D. (2008). Use of a multi-sensored AUV to telemeter tagged Atlantic sturgeon and map their spawning habitat in the Hudson River, USA. Autonomous Underwater Vehicles, 2008. AUV 2008. IEEE/OES (pp. 1–7).

Hensor, E., Couzin, I. D., James, R., & Krause, J. (2005). Modelling density-dependent fish shoal distributions in the laboratory and field. Oikos, 110(2), 344–352.

Hilborn, R. (1990). Determination of fish movement patterns from tag recoveries using maximum likelihood estimators. Canadian Journal of Fisheries and Aquatic Sciences, 47(3), 635–643.

Humphries, N. E., Queiroz, N., Dyer, J. R. M., Pade, N. G., Musyl, M. K., Schaefer, K. M., Fuller, D. W., Brunnschweiler, J. M., Doyle, T. K., Houghton, J. D. R., et al. (2010). Environmental context explains levy and Brownian movement patterns of marine predators. Nature, advance on (7301), 1066–1069.

Huse, G., Railsback, S., & Feron, A. (2002). Modelling changes in migration pattern of herring: Collective behaviour and numerical domination. Journal of Fish Biology, 60(3), 571–582.

Johnson, A. R., Wiens, J. A., Milne, B. T., & Crist, T. O. (1992). Animal movements and population dynamics in heterogeneous landscapes. Landscape Ecology, 7, 63–75.

Jonsen, I. D., Flemming, J. M., & Myers, R. A. (2005). Robust stateÃ.space modeling of animal movement data. Ecology, 86(11), 2874–2880.

Katz, Y., Tunstrom, K., Ioannou, C. C., Huepe, C., & Couzin, I. D. (2011). Inferring the structure and dynamics of interactions in schooling fish. Proceedings of the National Academy of Sciences, 106(28), 1–6.

Kronhamn, T. (1998). Bearings-only target motion analysis based on a multihypothesis kalman filter and adaptive ownship motion control. In Radar, Sonar and Navigation, IEEE Proceedings (vol. 145–4, pp. 247–252), IEEE.

Lowe, C., & Bray, R. (2006). Movement and activity patterns. The ecology of marine fishes: California and adjacent waters (L. G. Allen, M. H. Horn, & D. J. Pondella, II) (Eds.), pp. 524–553, DOI: 10.1525/california/9780520246539.001.0001.

Lowe, C., & Goldman, K. (2001). Thermal and bioenergetics of elasmobranchs: Bridging the gap. In T. Tricas, & S. Gruber (Eds.), The behavior and sensory biology of elasmobranch fishes: An anthology in memory of donald richard nelson. The Netherlands: Kluwer Academic.

Lowe, C., Topping, D., Cartamil, D., & Papastamatiou, Y. (2003). Movement patterns, home range and habitat utilization of adult kelp bass (*paralabrax clathratus*) in a temperate notake marine reserve. Marine Ecology Progress Series, 256, 205–216.

Mason, T., & Lowe, C. (2010). Home range, habitat use, and site fidelity of barred sand bass within a Southern California marine protected area. Fisheries Research, 106, 93–101.

Morales, J. M., Haydon, D. T., Frair, J., Holsinger, K. E., & Fryxell, J. M. (2004). Extracting more out of relocation data: Building movement models as mixtures of random walks. Ecology, 85(9), 2436–2445.

Myers, R., Baum, J., Shepherd, T., Powers, S., & Peterson, C. (2007). Cascading effects of the loss of apex predatory sharks from a coastal ocean. Science, 315, 1846–1850.

Rife, J., & Rock, S. M. (2003). Segmentation methods for visual tracking of deep-ocean jellyfish using a conventional camera. IEEE Journal of Oceanic Engineering, 28(4), 595–608.

Schulz, D., Burgard, W., Fox, D., & Cremers, A. (2001). Tracking multiple moving targets with a mobile robot using particle filters and statistical data association. In Robotics and Automation, 2001. Proceedings 2001 ICRA. IEEE International Conference (vol. 2, pp. 1665–1670), IEEE.

Schulz, D., Burgard, W., Fox, D., & Cremers, A. (2003). People tracking with mobile robots using sample-based joint probabilistic data association filters. The International Journal of Robotics Research, 22(2), 99.

Sims, D., Southall, E., Richardson, A., Reid, P., & Metcalfe, J. (2003). Seasonal movements and behaviour of basking sharks from archival tagging: No evidence of winter hibernation. Marine Ecology Progress Series, 248, 187–196.

Sims, D. W., Humphries, N. E., Bradford, R. W., & Bruce, B. D. (2011). Levy flight and Brownian search patterns of a free-ranging predator reflect different prey field characteristics. Journal of Animal Ecology, 432–442.

Skalski, G. T., & Gilliam, J. F. (2000). Modeling diffusive spread in a heterogeneous population: A movement study with stream fish. Ecology, 81(6), 1685–1700.

Thrun, S., Burgard, W., & Fox, D. (2005). Probabilistic robotics. In Probabilistic Robotics (Intelligent Robotics and Autonomous Agents), MIT Press.

Thrun, S., Fox, D., Burgard, W., & Dellaert, F. (2001). Robust Monte Carlo localization for mobile robots. Artificial Intelligence, 128(1-2), 99–141.

Topping, D. T., Lowe, C., & Caselle, J. (2005). Home range and habitat utilization of adult california sheephead, *semicossyphus pulcher (labridae)*, in a temperate no-take marine reserve. Marine Biology, 147, 301–311.

Treptow, A., & Zell, A. (2004). Real-time object tracking for soccer-robots without color information. Robotics and Autonomous Systems, 48(1), 41–48.

Viswanathan, G. M., Buldyrev, S. V., Havlin, S., Da Luz, M. G., Raposo, E. P., & Stanley, H. E. (1999). Optimizing the success of random searches. Nature, 401(6756), 911–914.

Voegeli, F., Smale, M., Webber, D., & rade, Y., & O'Dor, R. (2001). Ultrasonic telemetry, tracking and automated monitoring technology for sharks. Environmental Biology of Fishes, 60(1), 267–282.

Zhou, J., & Clark, C. M. (2006). Autonomous fish tracking by ROV using monocular camera. Computer and Robot Vision, Canadian Conference, 0, 68.